JOURNAL OF GEOPHYSICAL RESEARCH, VOL. 113, B02306, doi:10.1029/2006JB004892, 2008

Mechanics of grain-size reduction in fault zones

Charles G. Sammis[1] and Yehuda Ben-Zion[1]

Received 5 December 2006; revised 15 August 2007; accepted 14 December 2007; published 22 February 2008.

[1] Recent observations of nanometer-scale particles in the cores of exhumed fault zones raise questions about how such small particles are formed and how they survive, especially if significant shear heating is produced during an earthquake. Commercial crushing and grinding operations encounter a grind limit near 1 μm below which particles deform plastically rather than fracturing. A fragmentation model and low-temperature plasticity mechanics indicate that it is not possible to produce under compressive loading and short timescale significantly smaller particles at any strain rate. However, shock loading and subcritical crack growth can produce nanometer-scale fragments in compression. Under tensile loading the fragment size is determined by a competition between the nucleation of cracks and stress relaxation in their neighborhoods. Therefore higher tensile strain rates produce smaller fragments. The ultimate limit is determined by the availability of elastic strain energy, which does not place a significant constraint on the minimum grain size. Grain growth kinetics suggests that survivability of grains is very temperature sensitive. A 10 nm quartz fragment will double its size in 0.1 s at 1000°C, in 20 s at 800°C, in 14 h at 600°C, and in 10 years at 400°C. The observation of grains smaller than 10 nm places meaningful constraints on the dynamic fields and permeability of the fault zone during a large earthquake. Microstructural analysis of the grains and rock damage may be used to infer whether fragmentation occurred under macroscopic tension or compression.

Citation: Sammis, C. G., and Y. Ben-Zion (2008), Mechanics of grain-size reduction in fault zones, *J. Geophys. Res.*, *113*, B02306, doi:10.1029/2006JB004892.

1. Introduction

[2] Earthquakes are commonly modeled as frictional instabilities on planar fault surfaces. However, real faults, some of which have been exhumed from seismogenic depths, show a more complex structure. Most displacement on large-scale faults appears to occur within a narrow (centimeters thick) ''core'' of extremely fine grained ultracataclasite containing one or more prominent slip surfaces that have accommodated most of the slip [e.g., *Sibson*, 2003; *Chester and Chester*, 1998]. The core is bordered by wider zones of fault gouge and breccia, typically meters thick, with particle sizes ranging from microns to centimeters and often having a power law size distribution [*Sammis et al.*, 1987]. The gouge and breccia zones are bordered, in turn, by fractured but cohesive wall rock in which the fracture density (damage) decreases to the regional background level over distances of several hundreds of meters [e.g., *Chester et al.*, 1993; *Wilson et al.*, 2003]. This basic structure seems to characterize many fault structures, although there are variations in the widths of the constitutive layers and in the degree of symmetry about the core [*Ben-Zion and Sammis*, 2003; *Biegel and Sammis*, 2004].

[3] There are two sets of questions that frame the fundamental motivations for detailed studies of fault zone structure. First, how does the structure form, and, more significantly, what information does it contain about the fields that were operative during prior earthquakes on the fault? For example, asymmetry in the damage structure of several strike-slip faults has been interpreted as indicating a preferred propagation direction of earthquake ruptures [e.g., *Ben-Zion and Shi*, 2005; *Dor et al.*, 2006a, 2006b]. The apparent absence of shear strain in the gouge and breccia have been interpreted as evidence that these zones are formed dynamically in the tensile field near the tip of a propagating earthquake rupture [*Brune*, 2001] and may be used to place constraints on the velocity of rupture propagation [*Reches and Dewers*, 2005].

[4] The second general motivation for studying fault zone structure is to understand how it affects the propagation of subsequent earthquake ruptures. For example, how much energy is expended as friction and fracture in the gouge and breccia compared to that dissipated as sliding friction on the fault plane [*Chester and Chester*, 2006]? Also, can we identify features of a fault zone that correspond to the heterogeneity (''asperities'' and ''barriers'') inferred by seismologists to nucleate and arrest earthquakes, and are earthquakes on a given fault section likely to have a preferred propagation direction?

[5] In this paper, we focus on the first set of questions, and, more specifically, we ask what can be learned about

[1]Department of Earth Sciences, University of Southern California, Los Angeles, California, USA.

0148-0227/08/2006JB004892$09.00

earthquake mechanics from the particle-size distributions? Since most cataclastic fault rocks are observed to have a band-limited power law (fractal) particle-size distribution, the characteristic parameters used to describe the distribution are the power (related to the fractal dimension) and the range of sizes over which the power law gives a good description (the upper and lower fractal limits). *Chester et al.* [2005] observed that particles in the ultracataclasite layer of the Punchbowl fault have a fractal distribution that extends from 40 μm down to 50 nm, with fragments below this lower fractal limit extending down to 4 nm. *Sammis and King* [2007] discuss the mechanisms that lead to fractal fragment distributions and how the fractal dimension is expected to evolve with increasing strain. Here we focus on the smallest observed fragment, which is often significantly smaller than the lower fractal limit. The smallest fragment size is interesting because the production of very small particles can place constraints on the mode (compression versus tension) and amplitude of the local stress field, as well as on the loading rate. The survival of very small particles may also place constraints on the amplitude and duration of the temperature pulse associated with the faulting. *Sleep* [1994] investigated the particle distribution that results from a steady state balance between fragmentation and the disappearance of small grains by Ostwald ripening in a hydrothermal environment. Here we focus on the mechanics of fragmentation that can produce nanometer-scale fragments and grain growth kinetics that allow them to survive.

[6] One intriguing observation is that many pulverized fault zone rocks appear to have been shattered in situ with little or no shear strain. While *Biegel et al.* [1989] have shown that it is possible to produce such fabric by slow quasi-static deformation, *Brune et al.* [1993] and *Reches and Dewers* [2005] proposed that this fabric was produced dynamically in the stress field at the rupture tip of an earthquake. Dynamic generation of fabric without shear structure may be aided by local tension and opening associated with a wrinkle-like slip pulse on a bimaterial interface [*Ben-Zion and Andrews*, 1998; *Ben-Zion*, 2001]. Analytical results for a dynamic slip pulse show [*Rice et al.*, 2005] that crack tip stresses are sufficient to produce dynamic fracture extending meters from the fault plane at the centroid depth of several large earthquakes. Uniaxial tension can be produced in a compressive field near the rupture tip even in the absence of an opening mode of rupture.

[7] In sections 2–8 we explore a range of fragmentation mechanisms that might operate under both compressive and tensile stresses in a fault zone and ask what limits the smallest fragment size in each. Our analysis of compressive loading is motivated by the observation of a "grind limit" below which the particle size cannot be reduced in commercial crushing and grinding processes [*Prasher*, 1987]. Particles smaller than the grind limit are observed to deform plastically, changing their shape rather than fragmenting into smaller particles. By comparing the flow law (strain rate versus stress) for low-temperature dislocation plasticity with the stress level required to activate a flaw comparable to the size of the particle, we derive a relation for the minimum strain rate required to fracture a particle of a specified size at a specified temperature. We then extend the analysis to include compressive fragmentation under shock loading conditions and possible grain-size reduction by subcritical crack growth. For the case of tensile loading the low-temperature plasticity does not limit the grain size. Rather, grain size appears to be limited by the initial flaw distribution, the loading rate, and the elastic strain energy.

2. Grind Limit in Compressive Fragmentation

[8] It has been known since the eighteenth century that smaller particles are stronger [*Timoshenko*, 1953], but the reason remained unclear until the role of flaws as stress concentrators was recognized [*Griffith*, 1920]. The stress required to activate a flaw increases as the inverse square root of its length, and since the length of a flaw is limited by the size of a particle, strength increases as the inverse square root of particle size. This observed scaling is known as the Hall-Petch law [see *Scholz*, 2002]. However, the increase in strength is ultimately limited by plastic yielding. There are many observations that particles with diameters on the order of 1 μm or less do not fracture under a slow compressive load but deform plastically. In the crushing and grinding industry this smallest particle is known as the "grind limit." No additional amount of crushing and grinding can produce smaller particles.

[9] *Kendall* [1978] explored this transition from brittle to ductile deformation using the idealized two-dimensional particle in Figure 1. The force required to extend the mode I fracture in this geometry is

$$F = \frac{b}{(1 - w/d)} \left(\frac{2EG_c d}{3} \right)^{1/2}, \tag{1}$$

where E is Young's modulus, G_c is the fracture energy, and w, b, and d are the sample dimensions shown in Figure 1. Note that the tensile driving force on the fracture approaches 0 as w approaches d, and the force required to drive the fracture increases without bound.

[10] When the particle is compressed, stress concentration at the point causes plastic flow until

$$F = Ybw, \tag{2}$$

where Y is the compressive yield stress. Substituting equation (2) into equation (1) gives

$$\frac{1}{Yd} \left(\frac{F}{b} \right)^2 - \left(\frac{F}{b} \right) + \left(\frac{2EG_c d}{3} \right)^{1/2} = 0. \tag{3}$$

[11] When d is large, the first term can be ignored, and the normal stress σ_1 required to fracture the particle is, as expected, proportional to the inverse square root of the particle size d

$$\sigma_1 = \frac{F}{bd} = \left(\frac{2EG_c}{3} \right)^{1/2} d^{-1/2} = (2/3)^{1/2} K_{Ic} d^{-1/2}, \tag{4}$$

where we have introduced the critical stress intensity factor for mode I rupture, $K_{Ic}^2 = EG_c$. As d becomes smaller, the

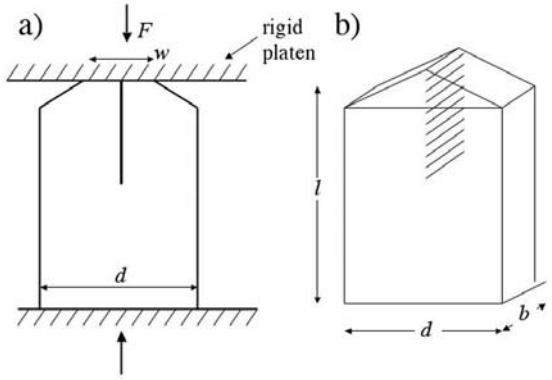

Figure 1. Prismatic particle geometry used by *Kendall* [1978] to estimate the minimum particle size that can be fractured in compression. (a) The loading configuration is shown. (b) A three-dimensional view of the sample is shown.

first term in equation (3) cannot be ignored. Solving the quadratic equation (3) for (F/b) as a function of d gives

$$\left(\frac{F}{b}\right) = \left(1 - \sqrt{1 - \frac{4(2/3)^{1/2} K_{Ic}}{Y\sqrt{d}}}\right) \frac{Yd}{2}. \tag{5}$$

[12] In terms of stress $\sigma_1 = \frac{F}{bd}$, equation (5) can be written as

$$\frac{\sigma_1}{\mu} = \frac{Y}{2\mu}\left(1 - \sqrt{1 - \frac{4(2/3)^{1/2} K_{Ic}}{Y\sqrt{d}}}\right), \tag{6}$$

where the stresses have been scaled by the shear modulus μ.

[13] Equation (6) implies a critical particle size d_{crit} below which σ_1 rises rapidly and fracture becomes impossible,

$$4\left(\frac{K_{Ic}}{Y}\right)\left(\frac{2}{3d_{\text{crit}}}\right)^{1/2} = 1 \tag{7}$$

or

$$d_{\text{crit}} = \frac{32}{3}\left(\frac{K_{Ic}}{Y}\right)^2. \tag{8}$$

[14] *Kendall* [1978] used crushing experiments on plastic samples in the shape depicted in Figure 1b to show that equation (6) gives a good description of the brittle-ductile transition. While the form of equation (1) is quite general, the numerical factor $\sqrt{2/3}$ depends on the geometry in Figure 1. We therefore replace $\sqrt{2/3}$ with a constant C that will be adjusted to fit crushing data on aluminum oxide spheres. Equations (6) and (8) thus become

$$\frac{\sigma_1}{\mu} = \frac{Y}{2\mu}\left(1 - \sqrt{1 - \frac{4CK_{Ic}}{Y\sqrt{d}}}\right) \tag{9}$$

$$d_{\text{crit}} = 16\left(\frac{CK_{Ic}}{Y}\right)^2. \tag{10}$$

[15] By fitting equations (9) and (10) to crushing data on aluminum oxide spheres we find that C is close to $\sqrt{2/3}$ and therefore not especially sensitive to grain shape. The important point is that the grind limit d_{crit} in equation (10) is very sensitive to the compressive yield stress Y, which itself is a function of temperature and loading rate. In section 3 we use this dependence to place a lower bound on the strain rate required under compressive loading to fracture a particle of a specified size at a specified temperature.

3. Low-Temperature Plasticity in Rock

[16] At low temperatures or high strain rates, crystalline solids deform by dislocation glide on a system of slip planes. *Ashby and Verrall* [1978] identified two thermally activated mechanisms that control the rate of such glide: lattice resistance–controlled glide and obstacle-controlled glide. Lattice resistance refers to the energy required to break interatomic bonds. An approximate flow law that fits data in this regime is given by *Ashby and Verrall* [1978] as

$$\dot{\gamma} = \dot{\gamma}_p \left(\frac{\sigma_s}{\mu}\right)^2 \exp\left\{-\frac{\Delta F_p}{kT}\left[1 - \left(\frac{\sigma_s}{\hat{\tau}_p}\right)^{3/4}\right]^{4/3}\right\}, \tag{11}$$

where $\dot{\gamma}_p$ is a constant, ΔF_p is the activation energy to break bonds, and $\hat{\tau}_p$ is the flow stress at 0 K. Note that σ_s is the shear stress that produces the strain rate $\dot{\gamma}$. It is related to the compressive yield strength in section 2 as $\sigma_s = Y/2$. Hence equation (11) relates compressive yield stress to strain rate.

[17] At higher temperatures lattice resistance drops, and dislocation glide is rate limited by discrete obstacles (like impurities or other dislocations) on the slip planes. When obstacles control the process, the flow is better described by [*Ashby and Verrall*, 1978]

$$\dot{\gamma} = \dot{\gamma}_o \exp\left\{-\frac{\Delta F_o}{kT}\left(1 - \frac{\sigma_s}{\hat{\tau}_o}\right)\right\}, \tag{12}$$

where $\dot{\gamma}_o$ is a constant, ΔF_o is the activation energy for cutting or passing the obstacle, and $\hat{\tau}_o$ is the flow stress at 0 K when the obstacles act alone. Table 1 summarizes values of the parameters in equations (11) and (12) for Al_2O_3 and olivine given by *Frost and Ashby* [1982] and *Ashby and Verrall* [1978].

[18] Figures 2 and 3 show the flow stress predicted by equations (11) and (12) for Al_2O_3 and for olivine as a function of the homologous temperature T/T_m for a range of strain rates $\dot{\gamma}$. The arc-shaped suite of curves at higher flow stress was generated using equation (11) for the case of lattice control. The narrow and nearly horizontal suite of curves was generated using equation (12) for the case of obstacle control. Note that the flow stress for obstacle control is almost independent of temperature and strain rate. As shown by *Ashby and Verrall* [1978], we assume that both lattice resistance and obstacles must be overcome and that the mechanism requiring the higher flow stress controls yielding at a given strain rate and temperature. For the high strain rates of interest here ($\dot{\gamma} \geq 1$), Figures 2 and 3 show that flow is rate limited by lattice control up to temperatures near the melting point in both Al_2O_3 and olivine. Unfortunately, even for the case of lattice-limited flow the flow stress is not very sensitive to the strain rate, especially at the

Table 1. Material Properties for α-Alumina and Olivine

Material Property	Symbol	Units	α-Alumina Al_2O_3	Olivine Mg_2SiO_4
Melting point at 1 atm	T_m	K	2320	2140
Burgers vector at 1 atm	b	m	4.76×10^{-10}	6.0×10^{-10}
Shear modulus at 300 K and 1 atm	μ	Pa	1.55×10^{11}	8.13×10^{10}
Flow stress at 0 K (lattice resistance)/modulus	$\frac{\hat{\tau}_p}{\mu}$	...	0.05	0.033
Preexponential for lattice resistance	$\dot{\gamma}_p$	s^{-1}	10^{11}	10^{11}
Activation energy for lattice resistance	$\frac{\Delta F_p}{\mu b^3}$	...	0.5	0.5
Flow stress at 0 K (obstacle control)/modulus	$\frac{\hat{\tau}_o}{\mu}$	...	5×10^{-3}	8×10^{-3}
Preexponential for obstacle control	$\dot{\gamma}_o$	s^{-1}	10^6	10^6
Activation energy for obstacle control	$\frac{\Delta F_o}{\mu b^3}$	...	0.5	0.5

small homologous temperatures we are interested in here. For example, a change in strain rate of 10 orders of magnitude in olivine at 300°C corresponds to only a factor of 2 change in flow stress (Figure 3). The change in flow stress is even less at lower temperatures.

4. Measured Compressive Strength of Al_2O_3 Microspheres

[19] Aluminum oxide microspheres provide a good test of the above model for compressive fragmentation and allow us to see if the constant C in equations (9) and (10) is sensitive to grain shape. Crushing strength data are available in the industrial literature since they are used in many commercial applications, and some of it has been plotted and referenced in Figure 4. The loading rate at which these strengths were determined is not reported, but it is not important. As we shall see, these particles are large enough to be in the inverse square root scaling regime which, according to equations (3) and (4), is independent of the compressive yield stress *Y. Yoshida et al.* [2005] have extended this data set to submicron particle sizes by using a modified hardness testing apparatus to measure the strength of Al_2O_3 particles with diameters near 0.7 μm. For these experiments the reported loading rate corresponds to a strain rate of $\dot{\gamma} \approx 10^{-4}$ s^{-1}. In Figure 5, which is an expanded portion of Figure 2, this strain rate at 300 K yields a flow stress of $\sigma_s/\mu = 0.031$, which corresponds to a compressive yield stress of $Y/\mu = 2\sigma_s/\mu = 0.062$. In Figure 4, experimental crushing strength data for Al_2O_3 spheres have been fit to equation (9) using $Y/\mu = 0.062$ and a geometrical constant $C = 0.7$. Because the particles measured by *Yoshida et al.* [2005] are so small, we chose to use the value of $K_{Ic} = 2.35$ MPa $m^{1/2}$ measured for single crystals. The value of K_{Ic} for polycrystalline aluminum oxide is larger with measurements covering the range from 3 to 5 MPa $m^{1/2}$ [*Ashby and Jones*, 2005]. Since K_{Ic} only appears as the product CK_{Ic} in equation (9), a larger value of K_{Ic} can be compensated by a smaller value of C without changing the theoretical curve in Figure 4. Our empirical value of $C = 0.7$ is slightly smaller than $C = \sqrt{2/3} = 0.82$ for the prismatic grain in Figure 1. The implication is that it takes slightly less force to fracture a spherical particle than a prismatic one, but this difference may not be significant in view of the uncertainty in the critical stress intensity factor and other material properties. The effect of fragment geometry on fracture strength appears to be small. The differences between the two commercial data sets may be due to

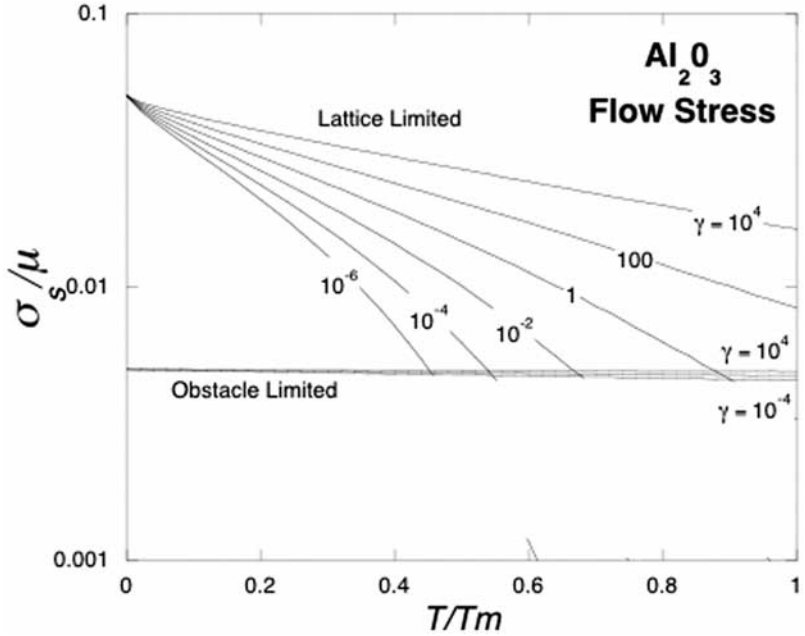

Figure 2. Deformation mechanism map for dislocation glide mechanism in aluminum oxide.

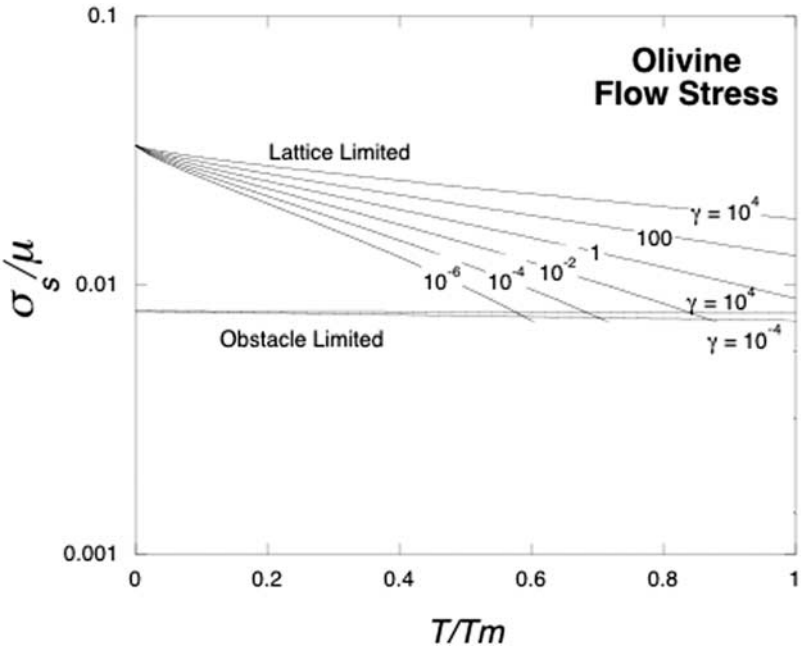

Figure 3. Deformation mechanism map for dislocation glide mechanism in olivine.

differences in K_{Ic} associated with the differences in purity. As expected, the data for the higher-purity microspheres are more consistent with those of *Yoshida et al.* [2005].

5. Minimum Grain Size as a Function of Temperature and Strain Rate in Compressive Loading

[20] Even though the flow stress in Figures 2 and 3 is not very sensitive to temperature or strain rate, we can determine an absolute minimum grain size that is independent of both temperature and strain rate. Note that the flow stress never exceeds its value at 0 K ($\hat{\tau}_p/\mu$ in Table 1) for any strain rate at any higher temperature. Hence the compressive yield stress never exceeds $Y_{\max} = 2\hat{\tau}_p$, and the absolute smallest fragment independent of temperature and strain rate from equation (10) is

$$d_{\min} = 16\left(\frac{CK_{Ic}}{2\hat{\tau}_p}\right)^2. \tag{13}$$

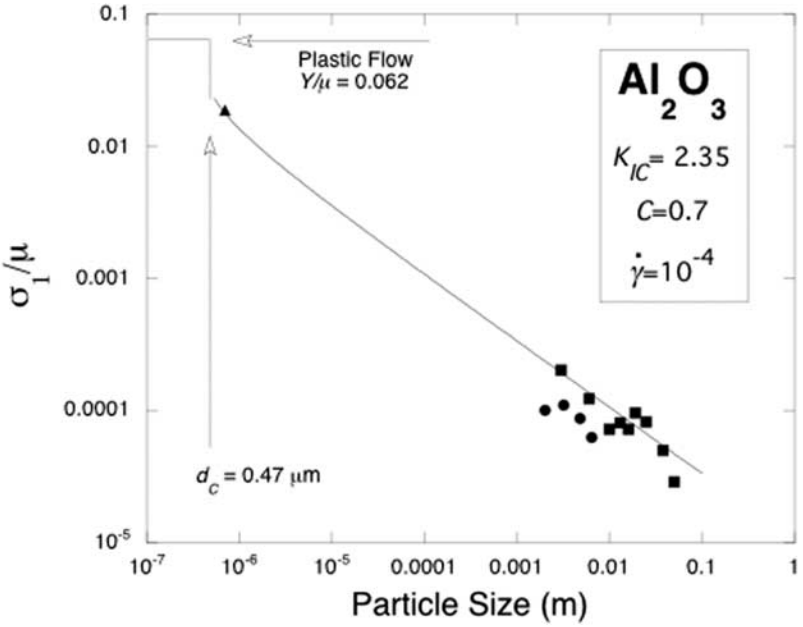

Figure 4. Crushing strength as a function of particle size for α-alumina spheres. The triangle is from *Yoshida et al.* [2005]. The circles are F-200 (93.1% pure) α-alumina spheres manufactured by Almatic AC, Inc., Houston, Texas. The squares are Denstone 99 (99+% pure) α-alumina spheres manufactured by Saint-Gobain Norpro, Stow, Ohio. The data are on the Web sites of these companies.

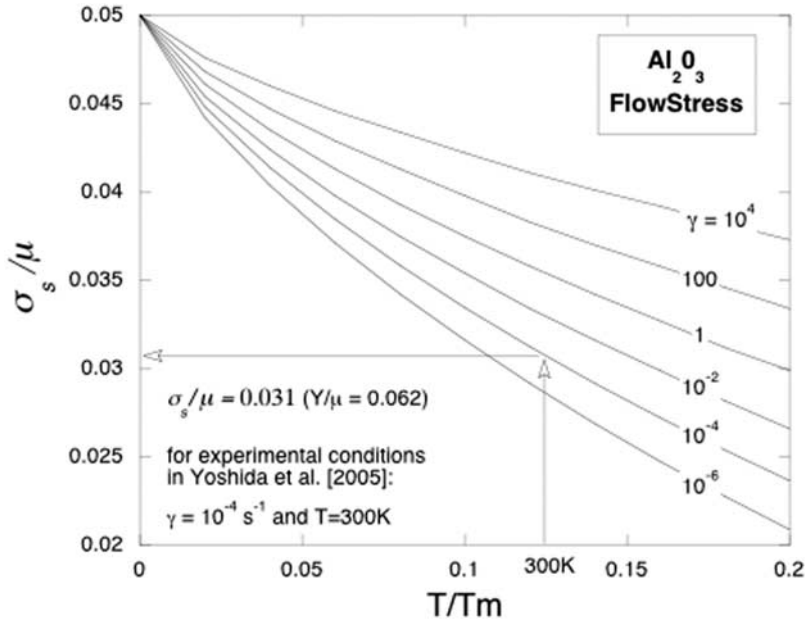

Figure 5. Deformation mechanism map used to estimate the flow stress at the experimental strain rate in the crushing strength tests of aluminum oxide microspheres by *Yoshida et al.* [2005].

[21] Equation (13) gives $d_{\min}$ = 180 nm for aluminum oxide and $d_{\min}$ = 268 nm for olivine. Although no deformation map exists for quartz, $\hat{\tau}_p$ cannot be larger than the ultimate lattice strength, which can be approximated as $\hat{\tau}_p \approx E/15$, where E = 71.7 GPa. Taking K_{Ic} = 1 MPa m$^{1/2}$ gives $d_{\min}$ = 86 nm for quartz. This is an extreme lower limit for slow compressive loading since $\hat{\tau}_p$ is probably a bit smaller for crystalline quartz. The implication is that quartz particles smaller than 86 nm could not have been produced in compression at any temperature or strain rate.

[22] Figure 6 shows the minimum strain rate required to fracture an olivine particle with diameter d as a function of temperature. The curves were calculated by solving equation (10) for the minimum shear stress required to fracture a particle of specified diameter d

$$\sigma_s = Y/2 = \frac{2CK_{Ic}}{\sqrt{d}} \tag{14}$$

and substituting this value of σ_s into equation (11) to find the corresponding strain rate.

6. Producing Nanometer Particles in Compression

[23] On the basis of the arguments thus far, the production of quartz fragments smaller than about 80 nm in compression seems impossible, and therefore the smaller fragments observed by *Chester et al.* [2005] must have been formed in tension. However, it may be possible to get around the size limit imposed by plastic deformation in two ways: by shock loading or by subcritical crack growth. Under shock conditions, stresses can be as much as 50 times higher than the flow stress [*Meyers*, 1994], which, according to equation (13), can reduce the minimum grain size by a factor of 2500, well below the nanometer scale.

[24] It may also be possible to produce smaller particles if the effective value of K_{Ic} is substantially reduced by stress corrosion. A limit to the effective K_{Ic} for subcritical crack growth in the presence of water has been very hard to demonstrate experimentally in silicates [*Scholz*, 2002] because of the very low crack velocities involved, which are typically $<10^{-9}$ m s^{-1}. *Atkinson* [1984] suggests that the effective K_{Ic} may be as low as 20% of its normal value. Note that a crack velocity of 10^{-9} m s^{-1} will split a 1 μm particle in only 1000 s or about 17 min. Comminution may thus occur in the wake of a large earthquake. Replacing K_{Ic} with 0.2 K_{Ic} in equation (13) reduces the minimum particle size to $d_{\min}$ = 11 nm for olivine and to $d_{\min}$ = 3 nm for quartz.

[25] Subcritical fragmentation may explain how *Yund et al.* [1990] were able to produce 10–15 nm particles in rotary shear experiments on granite. Stresses were compressive (the normal stress was 50–75 MPa), and the very low sliding velocities (10^{-3}–$10^{3.5}$ μm s^{-1}) rule out shock loading. They also produced up to 60% "amorphous material" that they argued was not quenched melt but might be composed of fragments too small to produce an X-ray signature. Their observation that the dislocation density in the resolvable particles was not above that in the original grains rules out significant plastic deformation during the comminution.

[26] *Scholz* [1987] has studied the accumulation of wear products generated during frictional slip, and one may consider the possibility that abrasion in the wear generation process may produce nanometer particles. However, the mechanics of wear is not significantly different from grain crushing. Both mechanisms involve fragmentation at points of stress concentration between asperities or grains, and

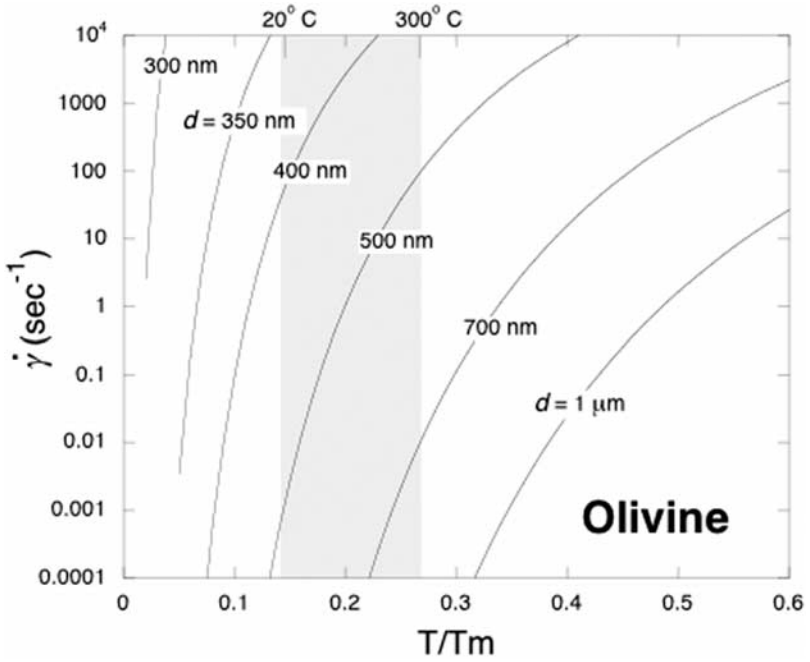

Figure 6. Minimum strain rate required to fracture an olivine particle of specified size at a given homologous temperature.

both are therefore subject to the same size limitations imposed by plastic yielding.

7. Fragmentation Under Tensile Loading

[27] *Rice et al.* [2005] found from fitting their analytic slip pulse model to the source parameters of several large earthquakes that uniaxial tension is developed within a few meters of the crack tip. An even larger tensile region is expected if there is an elastic contrast across the fault [*Andrews and Ben-Zion*, 1997; *Ben-Zion and Huang*, 2002]. Unlike compressive loading, fragmentation under tensile loading is not limited by ductile flow. Rather, the minimum particle size appears to be limited by a competition between the nucleation of tensile cracks and the subsequent relaxation of stress in their immediate vicinity. It is also possible that tensile fragmentation might be driven by local high temperatures and steep temperature gradients during flash heating on localized slip surfaces as discussed by *Rice* [2006]. We note that macroscopic tensile loading can only occur in a well-healed cataclasite, since an incohesive gouge would simply separate at the particle boundaries.

[28] The physics of tensile fragmentation is best illustrated by considering the one-dimensional expansion of a ring that contains a Poisson distribution of initial flaw spacing. Following each nucleation event, a domain of stress relaxation spreads bilaterally from the new crack at the elastic wave velocity $c = \sqrt{E/\rho}$, where E is the elastic modulus and ρ is the density. *Grady* [1981] derives the following expression for the resultant distribution of particle length L:

$$F(L) = \frac{2I_x}{\pi c}\left\{\exp\left[-\frac{I_x}{4c}L^2\right]\right\}\int_0^L\left\{\exp\left[-\frac{I_x}{4c}\zeta^2\right]\right\}d\zeta. \qquad (15)$$

[29] In this expression, I_x is the nucleation rate of regions of stress relaxation (twice the fracture nucleation rate) and is a function of the strain rate. The distribution is characterized by one parameter, a characteristic length $L^* = \sqrt{c/I_x}$, which reflects the competition between the nucleation rate and stress relaxation,

$$F(L) = \frac{2}{\sqrt{\pi}}\left(\frac{1}{L^*}\right)\exp\left[-\left(\frac{L}{2L^*}\right)^2\right]\mathrm{erf}\left(\frac{L}{2L^*}\right). \qquad (16)$$

[30] Equation (16) has a maximum value at $L/L^* = 1.24$. As the loading rate is increased, the nucleation rate I_x increases, the scaling length $L^* = \sqrt{c/I_x}$ decreases, and the most likely particle size also decreases. In the limit of shock loading, *Grady* [1981] shows that equation (16) can be written as

$$F(L) = N_o e^{-N_o L}, \qquad (17)$$

where N_o is the number of fractures (per unit length) that nucleate. The number of particles per unit length with $0 < L < L_{\min}$ is then

$$N(0 < L < L_{\min}) = N_o\int_0^{L_{\min}} N_o e^{-N_o L}dL = N_o\left(1 - e^{-N_o L_{\min}}\right), \qquad (18)$$

which gives for $N_o \gg 1$

$$L_{\min} = -\frac{1}{N_o}\ln\left(1 - \frac{1}{N_o}\right) \approx \frac{1}{N_o^2}.$$

[31] If $L_{\min}$ is 10 nm, then $N_o = 10^4$ fractures per meter. These results do not provide a useful constraint on the minimum size.

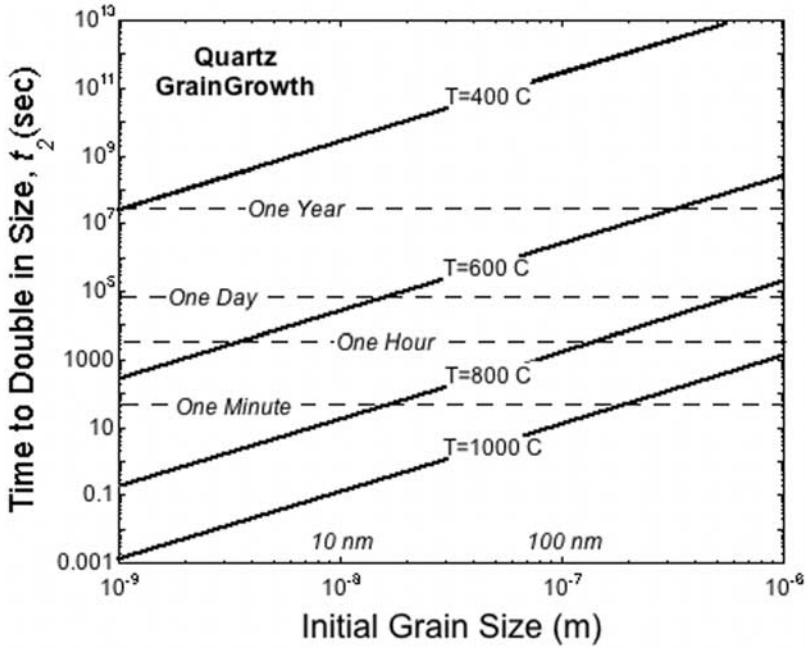

Figure 7. Time required to double the size of a quartz grain as a function of grain size at various temperatures.

[32] *Grady and Kipp* [1987] suggest that the extension of equation (17) to three-dimensional shock loading in tension can be written as

$$N(V) = N_o e^{-N_o V}. \quad (19)$$

[33] If we assume that each particle is a cube, then the surface area of a particle with volume V is $A(V) = 6V^{2/3}$. Since $N(V)$ is the number of particles between V and $V + dV$, the area of particles in this size range is $N(V)A(V)$, and the total area of the N_o particles is

$$A_{\text{tot}} = 6N_o^2 \int_0^\infty V^{2/3} e^{-N_o V} dV = 6N_o^{1/3}\Gamma(5/3) = 5.42N_o^{1/3}, \quad (20)$$

where the units of A_{tot} are area per unit volume and N_o is the number of particles per unit volume.

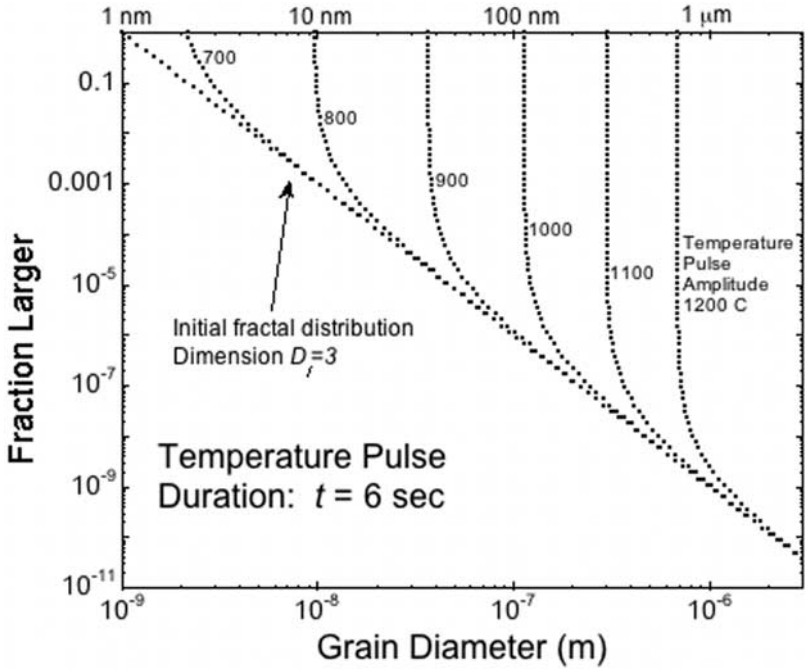

Figure 8. Effect of a temperature pulse with a 6 s duration and various amplitudes on an initially fractal distribution of fragments with dimension $D_f = 3$.

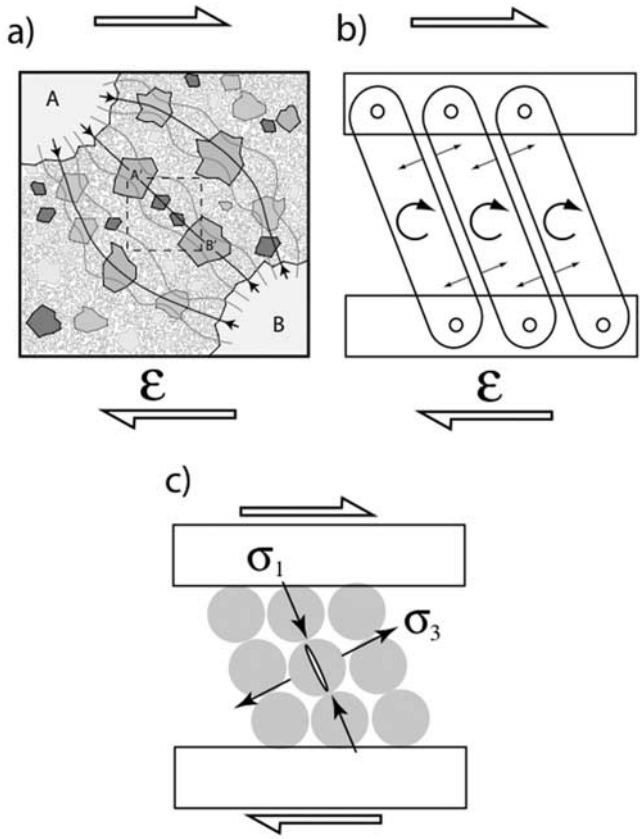

Figure 9. Schematic diagram of the fragmentation of gouge deformed in simple shear. (a) The stress is heterogeneous; the load is supported by grain bridges at all scales. (b) Grain bridges are idealized as beams. Rotation of a beam increases compression along its length while reducing compression across its width. (c) Grains that form the beam fail in tension. The failure plane is parallel to the long axis of the grain bridge and, because of the reduced compression across the bridge, tends to have its normal in the plane of Figure 9c (orthogonal to the intermediate principal stress σ_2). This anisotropy of failure planes is not expected when the tensile failure occurs in a global isotropic tensile field. Modified from *Sammis and King* [2007].

[34] The particle density is limited by the strain energy available to create the area A_{tot}. The required energy is $E_s = A_{\text{tot}}\gamma = A_{\text{tot}}(K_c^2/2E)$. For uniaxial elastic loading the elastic energy is $E_{el} = \sigma_1^2/2E$ so the maximum particle density is found by setting $E_s = E_{el}$, which gives $A_{\text{tot}}K_c^2 = \sigma_1^2$ or $N_o = (1/5.42)^3\,(\sigma_1/K_c)^6 = 0.0063(\sigma_1/K_c)^6$ particles per unit volume. Using a tensile stress of 5 GPa near the rupture front [*Reches and Dewers*, 2005] leads to $N_o = 0.0063(5000\text{ MPa}/1\text{ MPa m}^{1/2})^6 = 9.8 \times 10^{19}$ particles per cubic meter. The minimum particle size imposed by this energy constraint can be found using the volumetric equivalent of equation (18)

$$N(0 < V < V_{\min}) = N_o \int_0^{V_{\min}} N_o e^{-N_o V} dV = N_o\left(1 - e^{-N_o V_{\min}}\right) = 1, \tag{21}$$

which gives $L_{\min} \approx V_{\min}^{1/3} \approx 4 \times 10^{-14}$ m. The above considerations indicate that there is sufficient energy to make nanometer-sized particles in tension.

[35] Another way to look at this is to ask what is the smallest flaw that can be activated at a tensile stress of 5 GPa (calculated by *Reches and Dewers* [2005]) regardless of loading rate? For quartz this is given by $\sigma\sqrt{\pi a} = K_{Ic} = 1\text{ MPa m}^{1/2}$ (where a is the flaw radius), so $a_{\min} = (1/\pi)(10^6/5 \times 10^9)^2 = 13$ nm. If we assume that flaws in a given size range are uniformly distributed in the solid, then this would be the dimension of the smallest fragment. If, on the other hand, the initial flaws follow a Poisson or other nonuniform spatial distribution, even smaller fragments are possible.

8. Survivability of Nanometer-Sized Fragments

[36] The observation of nanometer-sized fragments in fault zone rocks also limits the amplitude and duration of the temperature pulse that was generated during the last earthquake. Simple grain growth in the absence of impurities and other structural complexities is commonly described by

$$L^2 - L_o^2 = C_o \exp\left[-\left(H + PV^*\right)/RT\right]t, \tag{22}$$

where L_o is the original grain size, L is the grain size after t seconds at temperature T in degrees Kelvin, H is the enthalpy, R is the universal gas constant, and pressure P is in pascals.

[37] For wet quartz, *Hacker et al.* [1992] give the following parameter values from laboratory work done by *Tullis and Yund* [1982] and *Pierce and Christie* [1987]: $C_o = 7.4 \times 10^{-4}\text{ m}^2\text{ s}^{-1}$, $H = 281$ KJ mol^{-1}, and $V^* = -1.86 \times 10^{-8}\text{ m}^3\text{ mol}^{-1}$. These values were used in equation (22) to produce Figure 7, which shows the time required to double the grain size as a function of the original grain size for a range of temperatures. For example, a 10 nm quartz particle will double its size in 0.1 s at 1000°C, in 20 s at 800°C, in 14 hours at 600°C, and in 10 years at 400°C. *Rice* [2006] estimated maximum temperature rises between 300°C and 1200°C for his thermal pressurization fault model, with the higher values corresponding to more heavily damaged wall rock that is not as effective in confining the heated water. See also *Bizzarri and Cocco* [2006a, 2006b]. The implication is that the observation of 10 nm particles in fault zone gouge constrains the temperature of an earthquake-generated heat pulse that lasts for a few tens of seconds to less than about 800°C. The survival of 5–10 nm particles in the rotary shear experiments by *Yund et al.* [1990] and the possibility that even smaller particles may survive to compose the "amorphous material" are consistent with their estimate of a very small temperature increase (0.02°C) during sliding.

[38] To get a better idea of how grain growth might affect the particle size distribution in a fault zone, suppose that the earthquake produces a fractal grain size distribution given by

$$N(L_o) = N(1)d^{-D_f}, \tag{23}$$

where $N(L_o)$ is the number of particles of (pregrowth) size $L_o \pm \Delta L_o$ and D_f is the fractal dimension. If L_o is measured in nanometers, then $N(1)$ is the number of particles with dimension $1 \pm \Delta L_o$ nanometers. The effect of an earth-

Figure 10. Morphology of mud cracks formed in the two-dimensional (2-D) isotropic tensile stress field in the shrinking mud as it dries. Note that the individual tensile cracks curve to intersect preexisting cracks at right angles because this is the orientation of the principal tensile axis near an existing crack. The faces of the resultant 2-D fragments tend to meet at right angles. There would be no preferred orientation of the fracture planes in a 3-D isotropic expansion. Image courtesy NASA, Visible Earth, http://www.earthscienceworld.org/images/imageuse.html.

quake-related temperature pulse of amplitude T and duration t is to change the dimensions of all the particles in the distribution according to equation (22). The new distribution is just $N(L) = N(L_o)$, with L given in terms of L_o by equation (22).

[39] To illustrate the above results for a case associated with a large earthquake, we assume that the earthquake rupture produces 6 m of slip over 6 s. Figure 8 shows how an initial fractal particle distribution with $D_f = 3$ is changed by a 6 s temperature pulse with amplitudes ranging from 750°C to 1200°C. Note that for $T > 800$°C, no particles smaller than 10 nm survive. The observation of 4 nm particles by *Chester et al.* [2005] implies that temperatures during a 6 s slip pulse on the slip surfaces of the Punchbowl fault never reached 800°C. In the context of the *Rice* [2006, Table 2] pore fluid heating model this temperature limit constrains the permeability in the core of the Punchbowl fault to be less than about 2×10^{-20} m^2.

9. Discussion and Conclusions

[40] Observations indicate that particles as small as 4 nm are observed in the fault zones of large displacement strike slip faults [e.g., *Chester et al.*, 2005]. We have shown that these particles are too small to have been formed by grain crushing in simple shear under elastic compressive loading, even at high strain rates. However, such small particles can be produced under compressive loading by either shock loading or, at the other extreme, by subcritical crack growth. The production of ~10 nm particles at low strain rates in compressive rotary shear [*Yund et al.*, 1990] is probably an example of such subcritical fragmentation.

[41] There appears to be no physical reason why nanometer-size particles cannot be produced under conditions of tensile loading at high strain rates. In such cases the grain size is limited by the competition between nucleation and local stress relaxation. For a nonuniform distribution of initial flaws the strain rate can always be made sufficiently high to nucleate closely spaced flaws and produce nanoscale particles. For a Poissonian distribution of initial flaws a tensile shock is expected to produce a particle distribution that increases exponentially toward small particles [e.g., see *Gilvarry*, 1961; *Gilvarry and Bergstrom*, 1961]. Energy limitations in this case allow particles smaller than 1 nm.

[42] The only constraint that the observation of submicron particles places on the comminution process is that it is probably not due to sequential grain crushing in compressive shear. Because of the effect of temperature on healing rates the survivability of nanoscale particles in fault zone structures requires a strong dynamic weakening mechanism to limit the amplitude and duration of the temperature pulse generated during earthquake ruptures.

[43] Careful analysis of the morphology of the grains and rock damage in fault zone structures may allow the distinction between fragmentation that occurred under macroscopic tension or compression. Tensile grain failure in an overall compressive shear field is likely to produce anisotropic structures in the gouge material because normal vectors to the fracture planes all tend to be orthogonal to the intermediated principal stress direction (Figure 9). To the extent

that the flow is simple shear, subsequent grain rotation will preserve this anisotropy. If, however, the grains are formed by the nucleation, growth, and intersection of tensile cracks in a macroscopic polyaxial tensile field, without significant shear displacement, the orientation of the fracture surfaces should be more random. In such cases the grains are likely to exhibit isotropic expansion, and the surfaces of the resultant fragments should meet at right angles, as illustrated by the mud crack pattern shown in Figure 10. Such patterns form because the principal tensile stress in isotropic tension is always parallel to an existing fracture. This pattern of orthogonal intersections can also be seen in crazed pottery glaze and the surface of old oil paintings. These expected differences in grain morphology should be observable in oriented orthogonal thin sections.

[44] Although this paper focuses on how the stress state during faulting may be inferred from the size and morphology of fault zone fragments, these constraints may be strengthened by other microscopic and macroscopic observations. For example, the observation of a fractal fragment size distribution may imply compressive shear where the fractal dimension provides an indication of total strain [*Sammis and King*, 2007]. Macroscopic features that may help to resolve the amplitude and type of the stress field operating during an earthquake rupture include injection structures and asymmetry of rock damage with respect to the principal slip surface [*Ben-Zion and Shi*, 2005; *Dor et al.*, 2006a, 2006b].

[45] **Acknowledgments.** This study was funded by the National Science Foundation (grant EAR-0510142) and the Southern California Earthquake Center (based on NSF cooperative agreement EAR-8920136 and U.S. Geological Survey cooperative agreement 14-08-0001-A0899). The manuscript benefited from comments by Judi Chester and an anonymous referee.

References

Andrews, D. J., and Y. Ben-Zion (1997), Wrinkle-like slip pulse on a fault between different materials, *J. Geophys. Res.*, *102*, 553–571.

Ashby, M. F., and D. R. H. Jones (2005), *Engineering Materials I: An Introduction to Properties, Applications and Design*, 3rd ed., Elsevier, Oxford, U. K.

Ashby, M. F., and R. A. Verrall (1978), Micromechanisms of flow and fracture, and their relevance to the rheology of the upper mantle, *Philos. Trans. R. Soc. London, Ser. A*, *288*, 59–93.

Atkinson, B. K. (1984), Subcritical crack growth in geological materials, *J. Geophys. Res.*, *89*, 4077–4114.

Ben-Zion, Y. (2001), Dynamic rupture in recent models of earthquake faults, *J. Mech. Phys. Solids*, *49*, 2209–2244.

Ben-Zion, Y., and D. J. Andrews (1998), Properties and implications of dynamic rupture along a material interface, *Bull. Seismol. Soc. Am.*, *88*, 1085–1094.

Ben-Zion, Y., and Y. Huang (2002), Dynamic rupture on an interface between a compliant fault zone layer and a stiffer surrounding solid, *J. Geophys. Res.*, *107*(B2), 2042, doi:10.1029/2001JB000254.

Ben-Zion, Y., and C. G. Sammis (2003), Characterization of fault zones, *Pure Appl. Geophys.*, *160*, 677–715.

Ben-Zion, Y., and Z. Shi (2005), Dynamic rupture on a material interface with spontaneous generation of plastic strain in the bulk, *Earth Planet. Sci. Lett.*, *236*, 486–496, doi:10.1016/j.epsl.2005.03.025.

Biegel, R. L., and C. G. Sammis (2004), Relating fault mechanics to fault zone structure, *Adv. Geophys.*, *47*, 65–111.

Biegel, R. L., C. G. Sammis, and J. H. Dieterich (1989), The frictional properties of a simulated gouge having a fractal particle distribution, *J. Struct. Geol.*, *11*, 827–846.

Bizzarri, A., and M. Cocco (2006a), A thermal pressurization model for the spontaneous dynamic rupture propagation on a three-dimensional fault: 1. Methodological approach, *J. Geophys. Res.*, *111*, B05303, doi:10.1029/2005JB003862.

Bizzarri, A., and M. Cocco (2006b), A thermal pressurization model for the spontaneous dynamic rupture propagation on a three-dimensional fault: 2. Traction evolution and dynamic parameters, *J. Geophys. Res.*, *111*, B05304, doi:10.1029/2005JB003864.

Brune, J. N. (2001), Fault-normal dynamic loading and unloading: An explanation for "non-gouge" rock powder and lack of fault-parallel shear bands along the San Andreas Fault, *Eos Trans. AGU*, *82*(47), Fall Meet. Suppl., Abstract S22B-0655.

Brune, J., S. Brown, and P. A. Johnson (1993), Rupture mechanism and interface separation in foam rubber models of earthquakes: A possible solution to the heat flow paradox and the paradox of large overthrust, *Tectonophysics*, *218*, 59–67.

Chester, F. M., and J. S. Chester (1998), Ultracataclasite structure and friction processes of the Punchbowl fault, San Andreas system, California, *Tectonophysics*, *295*, 199–221.

Chester, F. M., J. P. Evans, and R. L. Biegel (1993), Internal structure and weakening mechanisms of the San Andreas Fault, *J. Geophys. Res.*, *98*, 771–786.

Chester, J. S., and F. M. Chester (2006), Energy dissipation and damage generation in seismic fault zones, *Eos Trans. AGU*, *87*, Fall Meet. Suppl., Abstract T43A-1632.

Chester, J. S., F. M. Chester, and A. K. Kronenberg (2005), Fracture surface energy of the Punchbowl fault, San Andreas system, *Nature*, *437*, 133–136.

Dor, O., T. K. Rockwell, and Y. Ben-Zion (2006a), Geological observations of damage asymmetry in the structure of the San Jacinto, San Andreas and Punchbowl faults in southern California: A possible indicator for preferred rupture propagation direction, *Pure Appl. Geophys.*, *163*, 301–349.

Dor, O., Y. Ben-Zion, T. K. Rockwell, and J. Brune (2006b), Pulverized rocks in the Mojave section of the San Andreas Fault zone, *Earth Planet. Sci. Lett.*, *245*, 642–654.

Frost, H. J., and M. F. Ashby (1982), *Deformation-Mechanism Maps: The Plasticity and Creep of Metals and Ceramics*, Pergamon, New York.

Gilvarry, J. J. (1961), Fracture of brittle solids. I. Distribution function for fragment size in a single fracture (theoretical), *J. Appl. Phys.*, *32*, 391–399.

Gilvarry, J. J., and B. H. Bergstrom (1961), Fracture of brittle solids. II. Distribution function for fragment size in a single fracture (experimental), *J. Appl. Phys.*, *32*, 400–410.

Grady, D. E. (1981), Fragmentation of solids under impulsive stress loading, *J. Geophys. Res.*, *86*, 1047–1054.

Grady, D. E., and M. E. Kipp (1987), Dynamic rock fragmentation, in *Fracture Mechanics of Rock*, edited by B. K. Atkinson, pp. 429–475, Academic, London.

Griffith, A. A. (1920), The phenomenon of rupture and flow in solids, *Philos. Trans. R. Soc. London, Ser. A*, *221*, 163–198.

Hacker, B. R., A. Yin, J. M. Christie, and G. A. Davis (1992), Stress magnitude, strain rate, and rheology of extended middle continental crust inferred from quartz grain sizes in the Whipple Mountains, California, *Tectonics*, *11*, 36–46.

Kendall, K. (1978), The impossibility of comminuting small particles by compression, *Nature*, *272*, 710–711.

Meyers, M. A. (1994), *Dynamic Behavior of Materials*, John Wiley, New York.

Pierce, M. L., and J. M. Christie (2005), Kinetics and grain growth in quartz aggregates (abstract), *Eos Trans. AGU*, *68*(16), 4221987.

Prasher, C. (1987), *Crushing and Grinding Process Handbook*, 474 pp., John Wiley, New York.

Reches, Z., and T. A. Dewers (2005), Gouge formation by dynamic pulverization during earthquake rupture, *Earth Planet. Sci. Lett.*, *235*, 361–374.

Rice, J. R. (2006), Heating and weakening of faults during earthquake slip, *J. Geophys. Res.*, *111*, B05311, doi:10.1029/2005JB004006.

Rice, J. R., C. G. Sammis, and R. Parsons (2005), Off-fault secondary failure induced by a dynamic slip-pulse, *Bull. Seismol. Soc. Am.*, *95*, 109–134.

Sammis, C. G., and G. C. P. King (2007), Mechanical origin of power law scaling in fault zone rock, *Geophys. Res. Lett.*, *34*, L04312, doi:10.1029/2006GL028548.

Sammis, C. G., G. C. P. King, and R. Biegel (1987), The kinematics of gouge deformation, *Pure. Appl. Geophys.*, *125*, 777–812.

Scholz, C. H. (1987), Wear and gouge formation in brittle faulting, *Geology*, *15*, 493–495.

Scholz, C. H. (2002), *The Mechanics of Earthquakes and Faulting*, 2nd ed., Cambridge Univ. Press, Cambridge, U. K.

Sibson, R. (2003), Thickness of the seismic slip zone, *Bull. Seismol. Soc. Am.*, *93*, 1169–1178.

Sleep, N. H. (1994), Grain size and chemical controls on the ductile property of mostly frictional faults at low-temperature hydrothermal conditions, *Pure Appl. Geophys.*, *143*, 41–60.

Timoshenko, S. (1953), *History of the Strength of Materials*, p. 58, McGraw-Hill, London.

Tullis, J., and R. A. Yund (1982), Grain growth kinetics of quartz and calcite aggregates, *J. Geol.*, *90*, 301–318.

Wilson, J. E., J. S. Chester, and F. M. Chester (2003), Microfracture analysis of fault growth and wear processes, Punchbowl fault, San Andreas system, California, *J. Struct. Geol.*, *25*, 1855–1873.

Yoshida, M., H. S. Ogiso, S. Nakano, and J. Akedo (2005), Compression test system for a single submicrometer particle, *Rev. Sci. Instrum.*, *76*, 093905, doi:10.1063/1.2038187.

Yund, R. A., M. L. Blanpied, J. D. Weeks, and T. E. Tullis (1990), Observation and interpretation of microstructures in experimental fault gouges, *J. Geophys. Res.*, *95*, 15,589–15,602.

Y. Ben-Zion and C. G. Sammis, Department of Earth Sciences, University of Southern California, 3651 Trousdale Parkway, Los Angeles, CA 90089-0740, USA. (sammis@usc.edu)